Monthly Notices
of the
ROYAL ASTRONOMICAL SOCIETY

Mon. Not. R. Astron. Soc. **416,** 680–688 (2011) doi:10.1111/j.1365-2966.2011.19084.x

Herschel-Astrophysical Terahertz Large Area Survey: detection of a far-infrared population around galaxy clusters⋆

K. E. K. Coppin,[1,2]† J. E. Geach,[1,2] Ian Smail,[2] L. Dunne,[3] A. C. Edge,[2] R. J. Ivison,[4,5] S. Maddox,[3] R. Auld,[6] M. Baes,[7] S. Buttiglione,[8] A. Cava,[9] D. L. Clements,[10] A. Cooray,[11] A. Dariush,[6,10,12] G. De Zotti,[8,13] S. Dye,[6] S. Eales,[6] J. Fritz,[7] R. Hopwood,[10] E. Ibar,[4] M. Jarvis,[14,15] M. J. Michałowski,[5] D. N. A. Murphy,[2] M. Negrello,[16] E. Pascale,[6] M. Pohlen,[6] E. Rigby,[3] G. Rodighiero,[17] D. Scott,[18] S. Serjeant,[16] D. J. B. Smith,[14] P. Temi[19] and P. van der Werf[5,20]

[1]*Department of Physics, McGill University, Ernest Rutherford Building, 3600 Rue University, Montréal, Québec H3A 2T8, Canada*
[2]*Institute for Computational Cosmology, Durham University, South Road, Durham DH1 3LE*
[3]*School of Physics and Astronomy, University of Nottingham, University Park, Nottingham NG7 2RD*
[4]*UK Astronomy Technology Centre, Royal Observatory, Blackford Hill, Edinburgh EH9 3HJ*
[5]*SUPA, Institute for Astronomy, University of Edinburgh, Royal Observatory, Blackford Hill, Edinburgh EH9 3HJ*
[6]*School of Physics & Astronomy, Cardiff University, Queens Buildings, The Parade, Cardiff CF24 3AA*
[7]*Sterrenkundig Observatorium, Universiteit Gent, Krijgslaan 281 S9, B-9000 Gent, Belgium*
[8]*INAF – Osservatorio Astronomico di Padova, Vicolo dell'Osservatorio 5, I-35122 Padova, Italy*
[9]*Departamento de Astrofísica, Facultad de CC. Físicas, Universidad Complutense de Madrid, E-28040 Madrid, Spain*
[10]*Astrophysics Group, Physics Department, Blackett Lab, Imperial College, Prince Consort Road, London SW7 2AZ*
[11]*Department of Physics and Astronomy, University of California, Irvine, CA 92697, USA*
[12]*School of Astronomy, Institute for Research in Fundamental Sciences (IPM), PO Box 19395-5746, Tehran, Iran*
[13]*SISSA, Via Bonomea 265, I-34136 Trieste, Italy*
[14]*Centre for Astrophysics Research, Science & Technology Research Institute, University of Hertfordshire, Hatfield, Herts AL10 9AB*
[15]*Physics Department, University of the Western Cape, Cape Town 7535, South Africa*
[16]*Department of Physics & Astronomy, The Open University, Milton Keynes MK7 6AA*
[17]*Dipartimento di Astronomia, Universita di Padova, Vicolo Osservatorio 2, I-35122 Padova, Italy*
[18]*Department of Physics and Astronomy, University of British Columbia, 6224 Agricultural Road, Vancouver, BC V6T 1Z1, Canada*
[19]*Astrophysics Branch, NASA Ames Research Center, MS 245-6, Moffett Field, CA 94035, USA*
[20]*Leiden Observatory, Leiden University, PO Box 9513, NL-2300 RA Leiden, the Netherlands*

Accepted 2011 May 16. Received 2011 May 11; in original form 2011 February 14

ABSTRACT

We report the detection of a significant excess in the surface density of far-infrared sources from the *Herschel*-Astrophysical Terahertz Large Area Survey within ∼1 Mpc of the centres of 66 optically selected clusters of galaxies in the Sloan Digital Sky Survey with $\langle z \rangle \sim 0.25$. From the analysis of the multiwavelength properties of their counterparts we conclude that the far-infrared emission is associated with dust-obscured star formation and/or active galactic nuclei (AGN) within galaxies in the clusters themselves. The excess reaches a maximum at a radius of ∼0.8 Mpc, where we find $1.0 \pm 0.3\,S_{250} > 34$ mJy sources on average per cluster above what would be expected for random field locations. If the far-infrared emission is dominated by star formation (as opposed to AGN) then this corresponds to an average star formation rate of $\sim 7\,M_{\odot}\,yr^{-1}$ per cluster in sources with $L_{IR} > 5 \times 10^{10}\,L_{\odot}$. Although lensed sources make a negligible contribution to the excess signal, a fraction of the sources around the clusters could be gravitationally lensed, and we have identified a sample of potential cases of cluster-lensed *Herschel* sources that could be targeted in follow-up studies.

Key words: gravitational lensing: strong – galaxies: clusters: general – galaxies: evolution – galaxies: starburst – submillimetre: galaxies.

⋆*Herschel* is an ESA space observatory with science instruments provided by European-led Principal Investigator consortia and with important participation from NASA.

†E-mail: coppink@physics.mcgill.ca

1 INTRODUCTION

The intimate connection between galaxies' environments and their star formation histories is evident in the evolution of the cluster galaxy stellar mass function (e.g. Vulcani et al. 2011). The most massive galaxies in rich clusters today appear to have been in place in progenitor environments since at least $z \sim 1$ (de Propris et al. 1999; Kodama & Bower 2003; Neistein, van den Bosch & Dekel 2006), and there has been little evolution in the number density of the most massive elliptical galaxies in the intervening 8 Gyr (Balogh et al. 2001). However, significant stellar mass evolution is still required in the remainder of the cluster population during this period (Balogh et al. 2001). The key features of this evolution are (a) a steepening of the faint end towards $z = 0$, i.e. low-mass end of the luminosity function (Stott et al. 2007); and (b) the appearance of a population of passive, massive lenticular (S0) galaxies in the cores of clusters since $z \sim 0.5$ (Dressler et al. 1997).

The increase in the fraction of low-mass galaxies can be explained by the continuous accretion of satellite galaxies (with subsequent gas stripping and the cessation of further cooling preventing further growth). The formation of S0s can only be accounted for in an evolutionary sequence connecting distant gas-rich discs undergoing a period of additional star formation to build up the total stellar mass and enhancement of bulge-to-disc ratios (Poggianti et al. 1999; Kodama & Smail 2001). Until relatively recently, evidence for the large star formation rates (SFRs) required for such a transformation in the spiral populations of intermediate-redshift clusters was lacking. However, since the advent of sensitive mid- and (now) far-infrared panoramic surveys, several studies have now revealed a population of hitherto optically hidden star-forming galaxies in rich clusters over $0.3 \lesssim z \lesssim 1.5$ (e.g. Duc et al. 2000, 2004; Fadda et al. 2000; Metcalfe et al. 2003; Geach et al. 2006; Finn et al. 2010; Kocevski et al. 2010; Braglia et al. 2011).

It has become clear that these obscured star-forming galaxies could be responsible for strong evolution in the stellar mass function of even rich clusters since $z \sim 0.5$. Thus, not only does this population provide a key insight into various environmental effects on the star formation histories of relatively 'normal' galaxies, but it also represents an important stage in the overall shaping of the galaxy population today. The globally averaged total SFR in rich clusters as well as the average field has been in strong decline since $z \sim 0.5$, although it is unclear how the strength of the evolution is tied to galaxies' environments. Indeed infrared studies have revealed significant variation in the SFRs of individual clusters (Geach et al. 2006). It is thought that the origin of this variation could be rooted in the different environmental conditions specific to different clusters, such as substructure, dynamical state, thermodynamic properties of the intracluster medium (ICM), etc. The next step in understanding this variation, and building up a more statistical picture of the evolution of the obscured star-forming populations of clusters since $z \sim 0.5$, is to turn to wide-field panoramic infrared surveys of a much larger sample of clusters and groups covering a large dynamic range of environment.

While previous surveys undertaken with *Spitzer* and the *Infrared Space Observatory* (*ISO*) have mapped the mid-infrared emission (e.g. 15–24 μm) of clusters, panoramic far-infrared surveys have so far been challenging. Both ground- and space-based surveys have lacked the field-of-view, sensitivity and resolution to cover large areas down to the required depths to pinpoint the obscured star-forming galaxy population (e.g. Wardlow et al. 2010). The *Herschel* space telescope (Pilbratt et al. 2010) has enabled us to move beyond these limitations (e.g. Rawle et al. 2010).

The *Herschel*-Astrophysical Terahertz Large Area Survey (H-ATLAS; Eales et al. 2010a) is the widest area submillimetre *Herschel*-Spectral and Photometric Imaging Receiver (SPIRE; Griffin et al. 2010) and Photodetector Array Camera and Spectrometer (PACS; Poglitsch et al. 2010) survey, and – when complete – will cover an area of $\sim$550 deg^2 from 100 to 500 μm. The large volume probed will contain a large number of galaxy clusters, and the sensitivity of the far-infrared observations will allow us to systematically search for obscured star-forming galaxies in their vicinity. This paper presents a statistical analysis of the *Herschel* SPIRE sources in the core of $0.07 < z < 0.43$ clusters as mapped by the Science Demonstration Phase (SDP) H-ATLAS observations, covering a $\sim$14.4 deg^2 field at 9 h (Ibar et al. 2010; Pascale et al. 2011). Our goals are twofold: (a) to search for *statistical* evidence of dust-obscured star formation activity in this cluster population; and (b) to identify any candidate cluster-lensed sources for further study and follow-up.

This paper is organised as follows: we describe our unique cluster detection algorithm and the H-ATLAS SDP SPIRE catalogue in Section 2, the statistical analysis and results of the H-ATLAS and cluster catalogue cross-correlation in Section 3, and summarize our findings in Section 4. Throughout we assume cosmological parameters from the *Wilkinson Microwave Anisotropy Probe* (*WMAP*) fits in Spergel et al. (2003): $\Omega_\Lambda = 0.73$, $\Omega_m = 0.27$ and $H_0 = 71\,\mathrm{km\,s^{-1}\,Mpc^{-1}}$.

2 CLUSTER AND H-ATLAS CATALOGUES

2.1 Cluster detection

We have used the technique presented in Murphy, Geach & Bower (2010) to identify clusters of galaxies from panoramic optical imaging. Briefly, the method uses a series of colour selections to first isolate 'red-sequence' cluster members (those where the 4000 Å break is bracketed by two filters), followed by the construction of a Voronoi diagram of the projected galaxy distribution. Clusters and groups are identified as associations of Voronoi cells, sharing at least one vertex between cells, with areas significantly lower (i.e. higher galaxy surface densities) than would be expected if the galaxies were randomly distributed on the sky. In this case we used photometry from the Sloan Digital Sky Survey (SDSS; York et al. 2000) 7th Data Release (DR7; Abazajian et al. 2009). For the selection, we employed Galactic extinction corrected MODELMAG in the $(g - r)$, $(r - i)$ and $(i - z)$ bands; see Gunn et al. (1998) for a description of the SDSS photometric system. The minimum number of 'connected' galaxies that qualify as a cluster is five. The position of the cluster core is defined as the average of the positions of the member galaxies' Voronoi cells, however, we also define a 'brightest cluster galaxy (BCG) centre' as the location of the brightest cluster member in the r band. Apertures placed on the cluster core defined by the geometric mean provide the most complete coverage of the member galaxies. We find 66 clusters within the H-ATLAS SDP coverage of $\simeq$14.4 deg^2. The redshifts of the clusters have been estimated from the photometric (and in some cases spectroscopic) redshifts of the cluster members (Abazajian et al. 2009). We note that 36 members out of a total of 549 galaxies across all clusters have spectroscopic redshifts from SDSS (6.5 per cent). For sources with spectroscopic redshifts, the mean spectroscopic-to-photometric redshift offset is -0.0018, with a standard deviation of 0.017. Further details can be found in Geach et al. (2011). The clusters span a redshift of 0.07–0.43 (85 per cent of the sample are at $0.15 \leq z \leq 0.35$) and have a median redshift of $\langle z \rangle = 0.25$ at

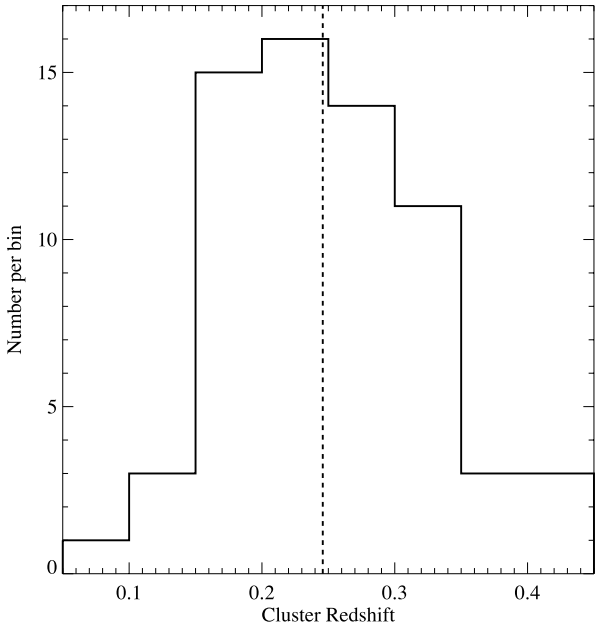

Figure 1. The redshift distribution of our 66-member cluster sample within the H-ATLAS SDP coverage of $\simeq$14.4 deg^2. We have estimated the cluster redshifts using the photometric (and for 6.5 per cent of the time spectroscopic) redshifts of the 549 cluster member galaxies (Abazajian et al. 2009). The clusters span a redshift of 0.07–0.43 (85 per cent of the sample are at $0.15 \leq z \leq 0.35$) and have a median redshift of $\langle z \rangle = 0.25$ (which we have indicated with a vertical dotted line) at which the angular scale is 240 kpc arcmin^{-1}.

which the angular scale is 240 kpc arcmin^{-1} (see Fig. 1). Based on tests performed on mock catalogues, the cluster catalogue is >90 per cent complete at a halo mass of 10^{14} M$_\odot$ (Murphy et al. 2010). The number of false positives can be estimated by randomly shuffling the colours of galaxies (while keeping the positions fixed) and re-running the detection algorithm. At the lower membership limit, the number of false detections is expected to be 0.06 deg^{-2} or <1 of the 66 clusters. Further details of the cluster algorithm, selection and completeness can be found in Murphy et al. (2010). We estimate the cluster richness using the commonly used $B_{\rm gc}$ statistic, an approximation of the amplitude of the real-space correlation function (Longair & Seldner 1979). Yee & Ellingson (2003) show that this statistical measure is reasonably well correlated with the physical properties of the clusters, and we apply these scalings to find the typical cluster scale R_{200}[1] $\simeq$ (1.2 $\pm$ 0.4) Mpc and $\log M_{200}/{\rm M}_\odot$[2] $\simeq$ (14.7 $\pm$ 0.5), although the errors on individual $B_{\rm gc}$ measurements are large.

2.2 The H-ATLAS SDP catalogue

The H-ATLAS SDP catalogue consists of 6876 sources detected at >5σ in either of the 250, 350 or 500 μm bands over a $\simeq$14.4 deg^2 region (Rigby et al. 2011). The 5σ point source sensitivity limits (including confusion noise) are 34, 38 and 44 mJy at 250, 350 and 500 μm, respectively. Smith et al. (2011) have employed a likelihood ratio (LR) method to perform the optical cross-identifications of the 6621 250-μm-detected sources with the SDSS DR7 catalogue with a limiting r-band magnitude of 22.4 (Abazajian et al. 2009). The LR technique assigns a reliability, R, to each match and indicates the probability that the counterpart is the correct identification. Of the 6876 H-ATLAS sources, 2423 are thus classified as having a reliable ($R \geq 0.8$) optical counterpart, and the remaining 4453 as optically unidentified ($R < 0.8$ or no optical counterparts).

[1] R_{200} is the equivalent radius enclosing a density ≥200 times the critical density.

[2] M_{200} is the mass within R_{200}.

3 ANALYSIS AND RESULTS

3.1 Measurement of far-infrared emission around the clusters

The first step of our analysis is to simply measure the surface density of H-ATLAS sources (both optically identified and unidentified) as a function of projected clustocentric radius around the 66 clusters (Fig. 2). As a field control sample, we repeat this exercise 1000 times for a set of 66 random positions across the field. As expected, at large radii the surface density around the clusters is indistinguishable from the average 'field' estimate, however, there is a clear positive excess of far-infrared sources within ∼5 arcmin (1.2 Mpc for $z = 0.25$) of the clusters, the significance of which peaks at ∼3.5 arcmin. There is an average excess of ∼one source per cluster over the background, although note that by definition the cluster environments are characterized by an excess surface density of galaxies. The total number of H-ATLAS sources detected within

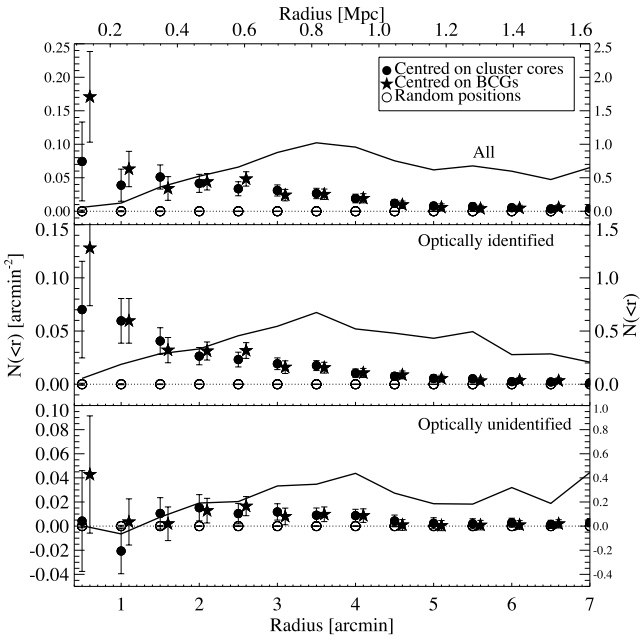

Figure 2. Cumulative number density of the average background-subtracted (points; axis on the LHS) and number (curve; axis on the RHS) of all (top panel), optically identified (middle panel) and optically unidentified (bottom panel) H-ATLAS sources as a function of clustocentric radius. For comparison, we have also plotted the average (background-subtracted) cumulative surface density as a function of radius from the central BCG (stars). The standard error of the mean has been used to calculate the error bars. This plot shows that we have measured an excess of H-ATLAS sources (with the significance varying with radius) within a projected clustocentric radius of 5 arcmin (which corresponds to 1.2 Mpc at $z = 0.25$) over that of the background field H-ATLAS sources, with optically identified sources (presumably far-infrared-bright cluster members, see text) making the most significant contribution to the measured excess. For reference, the average area of a single cluster is 7.5 arcmin^2, where the area is defined to contain 80 per cent of the cluster members originally assigned by the Voronoi tessellation detection.

3.5 arcmin of the 66 clusters is 401, representing a $\simeq 3.5\sigma$ excess of 67 ± 20 sources (the error is Poisson) above the background signal of 332 ± 1 sources on average (the error is the standard error of the mean). At a radius of 5 arcmin from the 66 clusters, we find 719 sources (a less significant excess of 41 ± 27 sources over our Monte Carlo estimated background signal of 678 ± 1 at the same clustocentric radius). For comparison, we have also repeated the above analysis using the projected radius from the BCG as the cluster centre, and the signal in the $r < 0.5$ arcmin bin clearly increases (see Fig. 2) – with six H-ATLAS sources lying within 8 arcsec of BCGs (note that the 250 μm point spread function is 19 arcsec). This suggests that several H-ATLAS sources are associated with the BCGs, either by lensing a background far-infrared source or that the far-infrared emission is from the BCG itself, e.g. Edge et al. (2010). We have quantified the likelihood of finding this excess signal by chance by using our Monte Carlo simulations and find that for radii $\lesssim$3.5 arcmin (where the maximum excess signal occurs) we would expect to see our average detected surface density <0.1 per cent of the time in randomly sampled apertures of equivalent size in the field. The simulations also reveal that at radii larger than about 5 arcmin the random chance of detecting our measured surface density (or greater) near the clusters above the background becomes >1 per cent and increases rapidly beyond 5 arcmin. Thus, for the following statistical analyses we use the 719 H-ATLAS sources found within 5 arcmin of the 66 clusters, which strikes a good balance of identifying the majority of the sources responsible for the excess signal while keeping the background field contribution to the signal to a minimum.

We have calculated the surface density of H-ATLAS sources in angular bins, regardless of the individual cluster redshift. An alternative approach would be to calculate the surface density as a function of physical projected radius, which would be important for broad redshift distributions. We conducted such an analysis as a check, by counting H-ATLAS sources within variable angular radii corresponding to a particular physical scale around the clusters. We calculate the field estimate using the same Monte Carlo technique as above, but using 66 apertures randomly drawn from a distribution function matching the cluster redshift distribution, repeating this 1000 times (see e.g. Temporin et al. 2009). The resulting surface density profile closely matches that found for angular bins, which is not surprising given our narrow redshift distribution (see Fig. 1), with the excess signal arising within $\simeq$1 Mpc of the cluster cores, in agreement with the 'average' physical scale shown in Fig. 2.

There are two distinct physical origins for the excess signal: (a) obscured star formation or active galactic nuclei (AGN) in cluster members; and (b) gravitational lensing of background sources. The majority of the H-ATLAS sources in low-redshift clusters are expected to have optical counterparts, whereas H-ATLAS sources with no robust counterpart are most likely to be at higher redshift (except in the case of galaxy–galaxy lensing, where the foreground lensing galaxy is identified as the counterpart). Splitting the sample into optically identified and unidentified subsamples therefore provides a crude method of determining if the excess signal seen around clusters comes from the cluster members themselves, or from strongly lensed background sources. From the 719 H-ATLAS sources found within 5 arcmin of the 66 clusters, we find that 268 (37 per cent) have optical counterparts with the remaining 451 (63 per cent) having no optical counterpart. To examine the relative contribution to the far-infrared excess signal, we repeat the radial surface density analysis described above for these two subsamples separately. Fig. 2 shows that the majority of the excess signal seen in the full sample is due to the *optically identified* H-ATLAS sources; while the surface density of optically unidentified H-ATLAS sources around clusters is essentially statistically indistinguishable from the random field. We thus now focus our attention on the optically identified sources around the clusters and defer a discussion of the nature of the optically unidentified sources to Section 3.4.

3.2 Is the far-infrared excess physically associated with the clusters?

We have determined that the excess signal of far-infrared emission around the low-redshift cluster sample comes from H-ATLAS sources with robust optical counterparts. These could be cases where a foreground galaxy is lensing a background source (Negrello et al. 2010) (where the lensing galaxy is the optical counterpart of the H-ATLAS source), or the far-infrared emission is from the galaxy itself. Is there any evidence to suggest that the majority of the optically identified H-ATLAS sources have redshifts consistent with the clusters?

We now perform a test to search for evidence that the far-infrared colours of H-ATLAS sources around the clusters are consistent with the redshift of the clusters. The optical photometric redshifts of the optical counterparts of the H-ATLAS sources are not useful for reliably distinguishing galaxy–galaxy lensing from the cluster members, since it is likely that in the case of galaxy–galaxy lensing, a far-infrared source would be identified with the lensing galaxy instead of the true background lensed source (which would be too faint/obscured to be seen in the optical). Follow-up millimetre studies that can positively identify the molecular gas emission of the high-redshift source, unambiguously separating it in redshift space from the foreground galaxy, is arguably the best technique. In lieu of those data, we can crudely use the far-infrared colours as a rough redshift discriminator, since the 250, 350 and 500 μm bands sample near the dusty spectral energy distribution (SED) peak. Thus, following e.g. Amblard et al. (2010) we compare the S_{250}/S_{350} and S_{500}/S_{350} SPIRE colours of the optically identified versus unidentified H-ATLAS cluster-matched sources to test if the optically identified sources are more consistent with being lower redshift cluster members and the optically unidentified sources more consistent with being background or cluster-lensed higher redshift sources. We note that not of all the H-ATLAS sources have direct detections in all three SPIRE bands (and thus errors on the colours of those individual sources will be large). Additionally, we note that ∼27 per cent of the 500 μm sources are likely blends of multiple sources (within a relatively large beamsize of ∼35 arcsec), with their flux boosted by up to a factor of ∼2 (Rigby et al. 2011). We thus place more emphasis on the results involving the 250 μm flux densities, which should suffer less from these effects due to the relatively smaller beamsize (∼18 arcsec), but use the 500 μm flux densities as a consistency check.

We use a Kolmogorov–Smirnov (KS) test to compare the S_{250}/S_{350} and S_{500}/S_{350} colours of the optically identified subset of 268 cluster-matched H-ATLAS sources with the 451 optically unidentified cluster-matched H-ATLAS sources to search for evidence of any differences between the colour distributions that would hint at an overall redshift difference between the two samples. The KS test reveals that there is a $<1 \times 10^{-8}$ chance that they are drawn from the same distribution. The optically identified cluster-matched H-ATLAS sources have bluer $\langle S_{250}/S_{350}\rangle = 1.88 \pm 0.06$ colours and bluer $\langle S_{500}/S_{350}\rangle = 0.4 \pm 0.02$ colours on average than the optically unidentified cluster-matched H-ATLAS sources ($\langle S_{250}/S_{350}\rangle = 1.3 \pm 0.03$; $\langle S_{500}/S_{350}\rangle = 0.5 \pm 0.01$). If we assume the median $3 \times 10^{10} < L_{\rm dust} < 10^{11}\,{\rm L}_{\odot}$ ultraviolet (UV)-submm template from

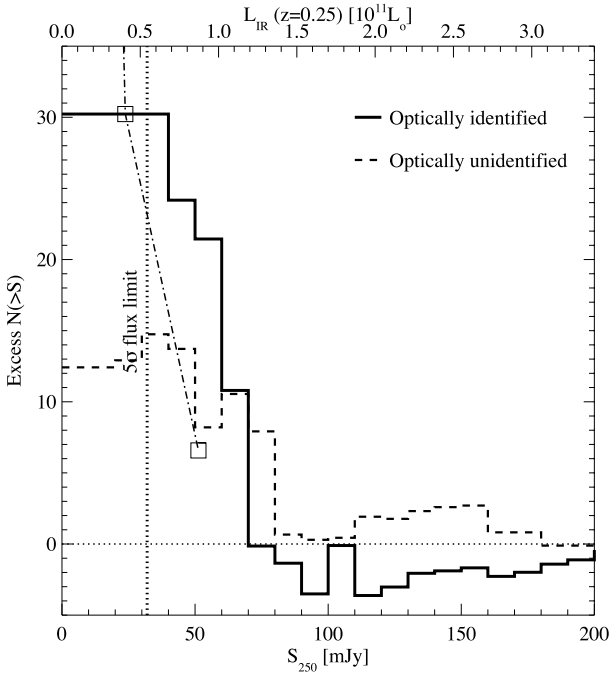

Figure 3. Background-subtracted cumulative number counts of optically identified and unidentified H-ATLAS sources within 5 arcmin of the 66 cluster cores. The 250 μm 5σ flux limit of the H-ATLAS catalogue is shown by the dotted vertical line. Based on the far-infrared colours, we expect most of the signal from the optically identified sources here to be cluster members (see text). As a guide, the upper scale corresponds to the total 8–1000 μm integrated luminosity, evaluated from the median $3 \times 10^{10} < L_{\rm dust} < 10^{11}$ $L_\odot$ UV-submm template from Smith et al. (in preparation) for a 'typical' H-ATLAS galaxy SED, redshifted to the median redshift of the cluster sample ($z = 0.25$) and normalized to the 250 μm flux. The $0.2 < z < 0.4$ HerMES submm luminosity function (square symbols connected with a dot–dash curve; Eales et al. 2010b) is overplotted for comparison and has been scaled arbitrarily to the bin at our survey flux limit.

Smith et al. (in preparation) for a 'typical' H-ATLAS galaxy SED, then these mean colours roughly indicate that the optically identified cluster-matched H-ATLAS sources, on average, lie at redshifts of $z \sim 0.25$ (consistent with the cluster redshifts) and that the optically unidentified sources are at typically higher redshifts of $z \sim 1$.

We thus conclude that the origin of the far-infrared excess signal around the clusters originates from sources within the clusters themselves. These galaxies are likely to be obscured star-forming galaxies or AGN. We note that although the actual AGN content of clusters as a function of time is still fairly poorly constrained, there is evidence that the infrared emission of the general cluster population (i.e. galaxies on the outskirts of clusters) is generated by star formation (Geach et al. 2009; Tomczak, Tran & Saintonge 2011).

We do expect some instances of galaxy–galaxy lensing in the optically identified sample. Cases of galaxy–galaxy lensing could potentially be enhanced around clusters simply due to the increased surface density of foreground galaxies, and the increased mass density cross-section in cluster regions can boost amplification further.[3] Therefore, a lensing galaxy may have a clear optical identification as a background source, but could be lensed further due to the presence of the cluster along the line of sight. We note that out of five instances of strongly lensed optically identified H-ATLAS sources identified by Negrello et al. (2010), one of these lies within 5 arcmin of a cluster core. This is strictly a lower limit on the occurrences of galaxy–galaxy lensing in our sample, however, the actual number of such cases is not expected to dominate the optically identified SPIRE sources in our sample, given their typical 500 μm fluxes and far-infrared colours described above.

[3] For example, although rare, the Cosmic Eye (Smail et al. 2007) is a $z \sim 3$ galaxy lensed in a near-perfect Einstein ring by a $z = 0.7$ elliptical that meets the threshold for strong lensing *only* because we are viewing the $z = 0.7$ galaxy through a foreground $z = 0.3$ cluster ∼1 arcmin away.

3.3 Integrated far-infrared emission from clusters at $z \sim 0.25$

If we now assume that the detected far-infrared emission is due to obscured star formation (as opposed to AGN) within the clusters then we can use the background-subtracted luminosity function to estimate the average level of star formation in the $z \sim 0.25$ clusters. We integrate a background-subtracted histogram of the 250 μm

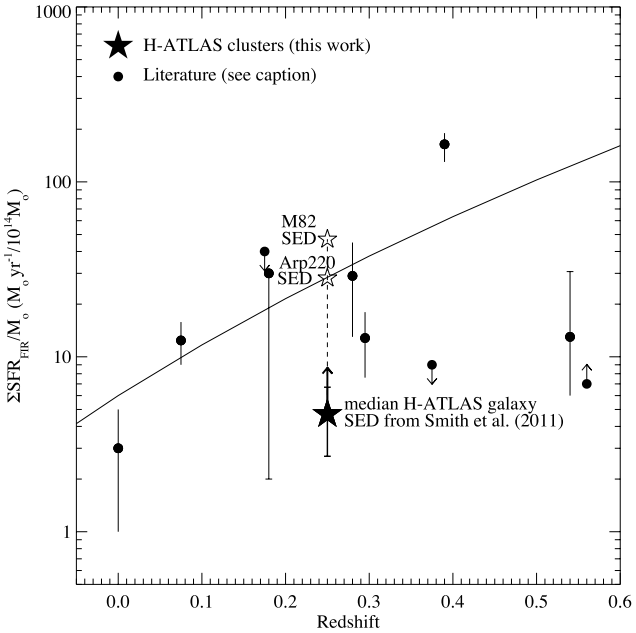

Figure 4. Measures of the mass-normalized SFRs in galaxy clusters out to $z \sim 0.6$, adapted from fig. 6 of Geach et al. (2006). The SFRs are derived from the mid- or far-infrared populations within ∼2 Mpc and are normalized to the best estimate of the total (luminous+dark) cluster mass. Listed in order of increasing redshift, they are Perseus (Meusinger, Brunzendorf & Krieg 2000), A3112 (Braglia et al. 2011), A2218 (Biviano et al. 2004), A1689 (Fadda et al. 2000; Duc et al. 2002), H-ATLAS (this work), A1758 (Haines et al. 2009), the Bullet cluster (Clowe, Gonzalez & Markevitch 2004; Markevitch 2006; Rawle et al. 2010), A370 (Metcalfe, Fadda & Biviano 2005), Cl 0024+16 and MS0451−03 (Geach et al. 2006) and J1888.16LC (Duc et al. 2004). An evolutionary model for the counts of star-forming ULIRGs from Cowie et al. (2004) is overlaid as a guide only, and has been normalized arbitrarily to the mean SFR in Cl 0024+16 and MS 0451−03 from Geach et al. (2006). This plot shows an increasing rate of activity in more distant clusters as traced through their mid- or far-infrared populations, albeit with a large scatter, suggestive that the infrared is a sensitive tracer of environmental changes within the clusters. Note that there are large systematic effects on the points in this plot, with the inferred SFR dependent on the assumed form of the SED, and estimate of the total cluster mass. Given the large uncertainties on the H-ATLAS cluster masses and the cool SED we have adopted, we consider our point a lower limit (as indicated by the arrow). We also show how our result changes if we instead assume an M82 or Arp 220 SED (open symbols), to facilitate a comparison with the literature results.

flux density of the optically identified cluster-matched H-ATLAS sources (see Fig. 3) to yield a total flux contribution of 1.6 Jy over the 66 clusters, or ∼24 mJy per cluster. Assuming this is a proxy for dusty star formation we can convert this to a total SFR by estimating the integrated total (8–1000 μm) infrared luminosity of the median H-ATLAS galaxy template with $3 \times 10^{10} < L_{\rm dust} < 10^{11}\,{\rm L}_{\odot}$ from Smith et al. (in preparation) redshifted to $z = 0.25$ (which is well matched to our sample far-infrared colours; see Section 3.2) and normalized to the relevant 250 μm flux density. We find an average SFR per cluster of $\sim 7 \pm 3\,{\rm M}_{\odot}\,{\rm yr}^{-1}$, applying the SFR calibration of 8–1000 μm integrated luminosity of Kennicutt (1998). The error range on the estimate represents the inferred difference in total luminosity within the redshift range of $0.2 < z < 0.3$. We note that a systematic uncertainty in the SFR estimate comes from our assumed SED, although this should not be a significant effect, since we have used an SED template based on the H-ATLAS galaxies themselves within this redshift range. Nevertheless, for example if an Arp 220 or M82 SED is assumed (which have been shown to be inappropriate for our sample; see Smith et al., in preparation) we find an SFR systematically higher by a factor of ∼6 or ∼10, respectively. The total SFR of the clusters should also be considered a lower limit, given the 250 μm sensitivity; since we only probe down to $L_{\rm IR} \sim 5 \times 10^{10}\,{\rm L}_{\odot}$, we also expect a contribution from dust-obscured galaxies below this limit. For example, assuming the shape of the *Herschel* Multi-tiered Extragalactic Survey (HerMES) 250 μm luminosity function (Eales et al. 2010b; see Fig. 3), if we could probe to a flux limit of ∼10 mJy we would expect an additional ∼90 sources down to $\sim 3 \times 10^{10}\,{\rm L}_{\odot}$, contributing an *additional* $\sim 7\,{\rm M}_{\odot}\,{\rm yr}^{-1}$ per cluster.

How does this compare to the total cluster-integrated SFR derived from the UV alone? To estimate the UV integrated SFR for the clusters, we evaluate the total SDSS *u*-band flux density within 5 arcmin of each cluster (corrected for Galactic extinction), and perform a field correction based on the total flux within randomly placed apertures across the field. We only sum the excess in galaxies not on the red sequence (as these are not present in the field), and derive an average total cluster integrated SFR of $\sim 20\,{\rm M}_{\odot}\,{\rm yr}^{-1}$, assuming the Kennicutt (1998) SFR calibration. Thus, the total UV-derived rate appears to be comparable to the total far-infrared-derived rate, but of course with the caveats that (a) the UV-derived value is likely integrated further down the cluster luminosity function due to higher sensitivity to star formation in lower mass systems, and indeed includes many galaxies with low activity missed by the far-infrared survey, (b) there is a large uncertainty in a simple conversion between the monochromatic *u* band to SFR and (c) we have not corrected for potentially non-negligible *u*-band emission from stars not associated with new star formation in red galaxies in the clusters (although we excluded the main red sequence).

With these caveats in mind, it is clear that the far-infrared-derived integrated SFR provides a superior estimate of the total level of star formation activity in the clusters, with the main uncertainty being the calibration of total far-infrared luminosity to SFR. However, it is also evident that the current limits of this H-ATLAS survey are missing part of the low-level activity in the clusters, as revealed by our simple UV estimates and extrapolation of the HerMES luminosity function. Our measurements should therefore be taken as lower limits to the integrated SFRs of these clusters, as mentioned previously.

If the total far-infrared-derived SFR of the clusters is normalized by total (luminous+dark) mass, we have a simple method to compare the activity in different environments, and the evolution of the cluster SFR budget over time (e.g. Geach et al. 2006). The mass estimates for these clusters are indirectly inferred from their optical richnesses (see Section 2.1), which gives the range ~ 1.5–$16 \times 10^{14}\,{\rm M}_{\odot}$ – however, the conversion between optical richness and mass is highly uncertain, and the true masses are likely to be at the lower end of this range. Even this might be an overestimate of the total cluster mass. For example, to achieve a similar surface density of clusters in the Millennium Simulation (Springel et al. 2005) requires us to be probing to a mass limit of $\log(M_{\rm halo}/{\rm M}_{\odot}) \gtrsim 13.5$.

Fig. 4 shows the average total SFR in our clusters compared to other infrared-derived rates in other clusters over $0 < z < 0.6$, although we note that given the large uncertainties on the H-ATLAS cluster masses and the cool SED we have adopted, we consider our point to be a lower limit. We note that if other infrared studies at similar redshifts and depths assume M82- or Arp 220-like templates for their cluster member galaxies when cooler H-ATLAS-type SEDs are more appropriate, then they may well be overestimating the level of star formation activity in those clusters. Although there

Table 1. A list of H-ATLAS strong lens candidates within 1 arcmin of cluster cores, ranked in order of decreasing 250 μm flux density (note that these particular sources are all detected at $\gtrsim 5\sigma$ at 250 μm). The mean colours of the lens candidates are typical of the colours of the optically unidentified H-ATLAS sources and are consistent with being high-redshift sources: $\langle S_{250}/S_{350}\rangle = 1.3 \pm 0.1$; $\langle S_{500}/S_{350}\rangle = 0.5 \pm 0.1$ (errors represent the error on the mean).

IAU identifier	SDP ID	RA (h m s)	Dec. (° ′ ″)	$r_{\rm c}$ (arcmin)	S_{250} (mJy)	S_{250}/S_{350}	S_{500}/S_{350}
HATLAS J091354.6−004539	SDP.219	09:13:54.7	−00:45:39.6	0.93	91.8 ± 6.7	1.1 ± 0.1	0.6 ± 0.1
HATLAS J090620.3+013112	SDP.535	09:06:20.3	01:31:12.1	0.91	72.4 ± 6.7	1.2 ± 0.2	0.6 ± 0.2
HATLAS J091130.9−002227	SDP.1445	09:11:30.9	−00:22:27.4	0.68	59.6 ± 6.9	1.2 ± 0.2	0.7 ± 0.2
HATLAS J090142.6+012128	SDP.1391	09:01:42.6	01:21:28.7	0.21	58.3 ± 6.7	1.2 ± 0.3	0.5 ± 0.2
HATLAS J091231.4−000703	SDP.1481	09:12:31.4	−00:07:03.5	0.67	56.9 ± 6.8	1.3 ± 0.3	0.4 ± 0.2
HATLAS J091149.4−000424	SDP.2331	09:11:49.4	−00:04:25.0	0.67	49.4 ± 6.8	1.8 ± 0.6	0.1 ± 0.3
HATLAS J091014.8−005024	SDP.2572	09:10:14.9	−00:50:24.4	0.43	48.2 ± 6.8	1.2 ± 0.3	0.5 ± 0.2
HATLAS J090405.7+014443	SDP.2249	09:04:05.7	01:44:43.22	0.30	46.8 ± 6.9	0.6 ± 0.1	0.8 ± 0.2
HATLAS J091233.8−004337	SDP.4357	09:12:33.9	−00:43:37.2	0.72	40.4 ± 6.8	1.2 ± 0.3	0.4 ± 0.3
HATLAS J091129.1−002237	SDP.4689	09:11:29.2	−00:22:37.4	0.21	37.8 ± 6.8	1.0 ± 0.3	0.7 ± 0.3
HATLAS J091309.6−003939	SDP.5079	09:13:09.6	−00:39:39.1	0.44	37.8 ± 6.8	1.7 ± 0.7	0.6 ± 0.5
HATLAS J090143.0+012224	SDP.5642	09:01:43.0	01:22:24.7	0.81	36.1 ± 7.0	2.6 ± 1.6	−0.2 ± 0.7
HATLAS J091342.4−004614	SDP.6622	09:13:42.5	−00:46:14.5	0.93	34.9 ± 6.8	1.3 ± 0.5	0.6 ± 0.4
HATLAS J090907.6−001209	SDP.7399	09:09:07.6	−00:12:09.9	0.89	33.4 ± 6.7	0.7 ± 0.2	0.8 ± 0.3

is significant cluster-to-cluster scatter, in general there has been strong evolution of the cluster SFR (see Geach et al. 2006). This is consistent with the scenario that there has been a sharper drop-off in the star formation activity of clusters since $z \sim 1$ than occurs in the field, probably related to the build up of virialized structures hostile to on-going activity and gas cooling over this period.

3.4 The nature of the optically unidentified far-infrared sources around the clusters

Although the optically unidentified sources within 5 arcmin of the clusters do not contribute significantly to the excess signal seen in Section 3.1 and appear to lie at typically higher redshifts ($z \sim 1$) on average than the optically identified H-ATLAS sources (Section 3.2) – these results suggest that strong gravitational lensing by the cluster potential is not a major contributor to the detected excess signal. Still, they represent an interesting sample, since they could contain strongly lensed galaxies. They thus provide potential opportunities to study the properties of intrinsically fainter far-infrared sources at high z than would otherwise be possible. It is possible that some of these galaxies could be galaxies at or below the cluster redshift, but are very highly obscured, although we note that Dunne et al. (2011) do not see evidence for a significant population of optically faint low-z sources. As a simple test for this, we consider a

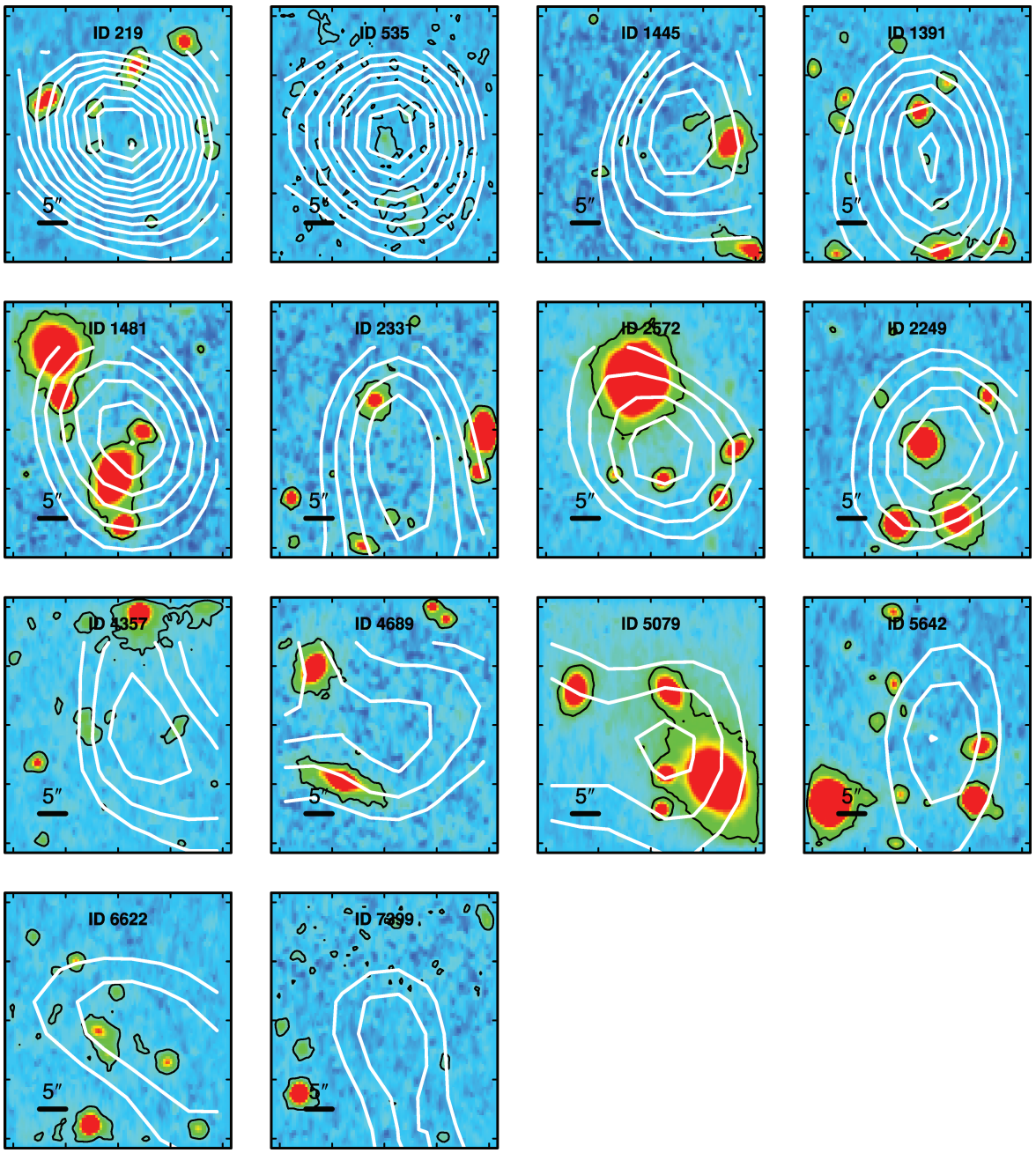

Figure 5. Co-added 40 × 40 arcsec^2 *gri* images of the 14 strong lens candidate H-ATLAS sources for further study and follow-up (centred on the 250 μm positions, with 250 μm contours starting at 3σ and increasing in steps of 1σ) within 1 arcmin (≃0.2 Mpc) of the cluster centres in order of decreasing 250 μm flux density (left–right, top–bottom).

prototypical ultraluminous infrared galaxy (ULIRG) with extreme reddening at UV–optical wavelengths: Arp 220 ($A_V > 15$ mag, with $A_V = 15$ mag in the most central 300 pc and much higher in the nuclei; Vermaas & van der Werf, in preparation). By redshifting this template to the cluster redshifts, and normalizing it to the observed 250 μm flux (the most sensitive band with the best angular resolution) we can assess whether we would have detected its optical counterpart by convolving the optical portion of the SED with, say, an *r*-band filter. If the predicted optical flux is above the limit of the observations of this field, then the galaxy would require even further extinction on top of the Arp 220 template or a different *k*-correction, implying a different (higher) redshift to the cluster. We find that all of the galaxies without current optical identifications are classified as high-*z* sources using this method, with predicted $r_{\rm SDSS}$ at least 1 mag brighter than the 22.4 mag SDSS limit. The 451 optically unidentified H-ATLAS sources are thus candidate lensed sources. Although the amplification factor falls off rapidly with radius for all sensible mass profiles, it is worth noting that the Einstein radius for these clusters is expected to be ∼20–40 arcsec for a mass range of 1–5 × 10^{14} $M_\odot$. Therefore, only a fraction of the 451 optically unidentified H-ATLAS sources are expected to be highly magnified.

Thus, from the 451 candidate lensed sources, we have singled out those sources lying within 1 arcmin (≃0.2 Mpc) of the cluster centres for further study, amounting to 14 strong lens candidates (see Table 1). The mean colours of the 14 lens candidates are typical of the colours of the optically unidentified H-ATLAS sources and are consistent with being high-redshift sources: $\langle S_{250}/S_{350}\rangle = 1.3 \pm 0.1$; $\langle S_{500}/S_{350}\rangle = 0.5 \pm 0.1$. In Fig. 5 we present co-added *gri* images of the sources, with 250 μm flux density contours overlaid.

4 SUMMARY AND CONCLUSIONS

We have detected a significant excess of optically identified far-infrared sources within ∼1.2 Mpc of the centres of optically selected clusters of galaxies with $\langle z\rangle \sim 0.25$ in the SDP H-ATLAS field. Assuming that the excess signal is completely dominated by star formation (rather than AGN), the far-infrared excess corresponds to an average SFR of ≈7 $M_\odot$ yr^{-1} per cluster.

The average cluster far-infrared SFR is consistent with mass-normalized SFRs from previous work. If the observed SFR in these clusters is maintained over the 3 Gyr since $z = 0.25$, then the activity could contribute ∼2 × 10^{10} $M_\odot$ of new stellar mass in the clusters – enough to construct a typical S0 bulge. Our average integrated SFR for the clusters can be considered a lower limit, since we expect additional contribution from obscured sources below the sensitivity limit of the H-ATLAS observations. This evolution is necessary for the observed increase in the fraction of massive (bulge dominated) lenticular galaxies in the cores of clusters over the same time period.

Finally, we have determined that the optically unidentified H-ATLAS sources within 5 arcmin (≃1.2 Mpc) of the cluster cores are higher redshift background sources, some of which could be strongly lensed by the cluster, and we have compiled a list of lensed candidates for further study. The future full H-ATLAS coverage will be sufficiently large that this analysis can be repeated and extended as a function of cluster redshift and mass. In addition, this analysis could be applied to targeted SPIRE observations of galaxy clusters.

ACKNOWLEDGMENTS

We thank the referee, Pierre-Alain Duc, for his suggestions which helped to improve the paper, and also Tracy Webb for useful discussions. KEKC and JEG acknowledge support from the endowment of the Lorne Trottier Chair in Astrophysics and Cosmology at McGill, the National Science and Engineering Research Council of Canada and the UK Science and Technology Facilities Council (STFC). KEKC also acknowledges the Centre of Research in Astrophysics of Québec for a fellowship. ACE, IS and RJI acknowledge support from STFC. GDZ acknowledges financial contribution from the agreement ASI-INAF I/009/10/0. The *Herschel*-ATLAS is a project with *Herschel*.

REFERENCES

Abazajian K. N. et al., 2009, ApJS, 182, 543
Amblard A. et al., 2010, A&A, 518, L9
Balogh M. L., Christlein D., Zabludoff A. I., Zaritsky D., 2001, ApJ, 557, 117
Biviano A. et al., 2004, A&A, 425, 33
Braglia F. G. et al., 2011, MNRAS, 412, 1187
Clowe D., Gonzalez A., Markevitch M., 2004, ApJ, 604, 596
Cowie L. L., Barger A. J., Fomalont E. B., Capak P., 2004, ApJ, 603, L69
de Propris R., Stanford S. A., Eisenhardt P. R., Dickinson M., Elston R., 1999, AJ, 118, 719
Dressler A., Oemler A., Jr, Butcher H. R., Gunn J. E., 1994, ApJ, 430, 107
Duc P.-A., Brinks E., Springel V., Pichardo B., Weilbacher P., Mirabel I. F., 2000, AJ, 120, 1238
Duc P.-A. et al., 2002, A&A, 382, 60
Duc P.-A. et al., 2004, in Diaferio A., ed., IAU Colloq. 195, Outskirts of Galaxy Clusters: Intense Life in the Suburbs. Astron. Soc. Pac., San Francisco, p. 347
Dunne L. et al., 2011, MNRAS, submitted (arXiv:1012.5186)
Eales S. et al., 2010a, PASP, 122, 499
Eales S. et al., 2010b, A&A, 518, L23
Edge A. C. et al., 2010, A&A, 518, L47
Egami E. et al., 2010, A&A, 518, L12
Fadda D., Elbaz D., Duc P.-A., Flores H., Franceschini A., Cesarsky C. J., Moorwood A. F. M., 2000, A&A, 361, 827
Finn R. A. et al., 2010, ApJ, 720, 87
Geach J. E. et al., 2006, ApJ, 649, 661
Geach J. E., Smail I., Moran S. M., Treu T., Ellis R. S., 2009, ApJ, 691, 783
Geach J. E., Murphy D. N., Bower R. G., 2011, MNRAS, 413, 3059
Griffin M. J. et al., 2010, A&A, 518, L3
Gunn J. E. et al., 1998, AJ, 116, 3040
Haines C. P., Smith G. P., Egami E., Okabe N., Takada M., Ellis R. S., Moran S. M., Umetsu K., 2009, MNRAS, 396, 1297
Ibar E. et al., 2010, MNRAS, 409, 38
Kennicutt R. C., 1998, ARA&A, 36, 189
Kocevski D. D. et al., 2010, ApJ, submitted (arXiv:1009.2750)
Kodama T., Bower R., 2003, MNRAS, 346, 1
Kodama T., Smail I., 2001, MNRAS, 326, 637
Longair M. S., Seldner M., 1979, MNRAS, 189, 433
Markevitch M., 2006, in Wilson A., ed., Proceedings of the X-ray Universe 2005, ESA SP-604. ESA, Noordwijk, p. 723
Metcalfe L. et al., 2003, A&A, 407, 791
Metcalfe L., Fadda D., Biviano A., 2005, Space Sci. Rev., 119, 425
Meusinger H., Brunzendorf J., Krieg R., 2000, A&A, 363, 933
Murphy D., Geach J. E., Bower R., 2010, MNRAS, submitted
Negrello M. et al., 2010, Sci, 330, 800
Neistein E., van den Bosch F. C., Dekel A., 2006, MNRAS, 372, 933
Pascale E. et al., 2011, MNRAS, doi:10.1111/j.1365-2966.2011.18756.x (arXiv:1010.5782)
Pilbratt G. L. et al., 2010, A&A, 518, L1
Poggianti B. M., Smail I., Dressler A., Couch W. J., Barger A. J., Butcher H., Ellis R. S., Oemler A., 1999, ApJ, 518, 576
Poglitsch A. et al., 2010, A&A, 518, L2
Rawle T. D. et al., 2010, A&A, 518, L14
Rigby E. E. et al., 2011, MNRAS, doi:10.1111/j.1365-2966.2011.19084.x (arXiv:1010.5787)
Smail I. et al., 2007, ApJ, 654, L33

Smith D. J. B. et al., 2011, MNRAS, in press (arXiv:1007.5260)
Spergel D. N. et al., 2003, ApJS, 148, 175
Springel V. et al., 2005, Nat, 435, 629
Stott J. P., Smail I., Edge A. C., Ebeling H., Smith G. P., Kneib J.-P., Pimbblet K. A., 2007, ApJ, 661, 95
Temporin S., Duc P.-A., Ilbert O., XMM-LSS/SWIR Collaboration, 2009, Astron. Nachr., 330, 915
Tomczak A. R., Tran K.-V. H., Saintonge A., 2011, ApJ, in press (arXiv:1105.0602)
Vulcani B. et al., 2011, MNRAS, 412, 246
Wardlow J. L. et al., 2010, MNRAS, 401, 2299
Yee H. K. C., Ellingson E., 2003, ApJ, 585, 215
York D. G. et al., 2000, AJ, 120, 1579

This paper has been typeset from a TEX/LATEX file prepared by the author.